Effect of rotation on mixing efficiency in homogeneous stratified turbulence using unforced direct numerical simulations

Matthew Klema[1,2] · S. Karan Venayagamoorthy[1] · Annick Pouquet[3,4] · Duane Rosenberg[5] · Raffaele Marino[6]

Abstract

Diapycnal (irreversible) mixing is analyzed using thirty direct numerical simulations (at 1024^3 resolution) of homogeneous rotating stratified turbulence (RST) in the absence of imposed shear or forcing. The influence of varied rotation and stratification rates on the energetics (in particular the dissipation rates of kinetic and potential energies) is presented. Data is also analyzed within a new parametric framework, using the turbulent Froude and Rossby numbers $Fr_t = \epsilon/Nk$, $Ro_t = \epsilon/fk$, where k is the turbulent kinetic energy, ϵ its rate of dissipation, N the buoyancy frequency and f the Coriolis parameter. This framework is used to illustrate relative magnitudes of the stratification and rotation in geophysical flows and provide a useful tool for explicating the relationship between Fr_t and Ro_t as relevant dynamic parameters in the geophysical setting. Results indicate that unforced rotation does not impact the magnitude of the irreversible mixing coefficient ($\Gamma = \epsilon_P/\epsilon$) when compared to results without rotation, where ϵ_P is the rate of potential energy dissipation. Moreover, it is shown that the recent scaling laws for mixing efficiency in stably stratified turbulence in the absence of rotation, as exemplified in Garanaik & Venayagamoorthy (*J. Fluid Mech.* 867, 2019, pp. 323-333), are applicable as well for homogeneous and decaying RST. Results also highlight the ambiguity of the ratio N/f as a control parameter for the classification of small-scale RST, and thus for evaluating diapycnal mixing.

Keywords Stratified turbulence · Rotation · Irreversible mixing · Oceanic turbulence

Matthew Klema, S. Karan Venayagamoorthy, Annick Pouquet, Duane Rosenberg and Raffaele Marino have contributed equally to this work.

✉ Matthew Klema
   mrklema@fortlewis.edu

Extended author information available on the last page of the article

2️ Springer

1 Introduction

The amount of energy available for mixing at small scales has many important implications for oceanic and atmospheric flows. Mixing in geophysical flows helps maintain the meridional overturning circulation and enters the estimations of the small-scale fluxes that are used in mass budgets, heat budgets and the mixing of nutrients [39]. Parameterizations of the eddy diffusivities of momentum (ν_t) and of the scalar density ($\kappa_{\rho t}$) are commonly used in large scale models, but models can be sensitive to the accuracy of the parameterization [14]. In order to be as accurate as possible these model parameterizations must account for all significant factors that influence mixing.

Density stratification is necessary for the existence of internal waves in the Earth's ocean and atmosphere, but the degree of stratification has a direct impact on the amount of diapycnal mixing [1]. A large body of work has analyzed turbulence and mixing in the presence of stratification (e.g. see [7, 16, 20, 21, 23, 26, 27, 29, 51, 52] and references therein). Another important factor in the analysis of geophysical flows is the impact of planetary rotation. It is less clear what impact rotation has on small scale turbulent mixing, especially in a role that is coupled with stratification [49]. The inclusion of rotation has led to increased study of inertia–gravity waves and what is classified as rotating stratified turbulence (RST)[9, 34, 35, 46, 55, 56]. For example, it was shown in Lindborg [28] that the direct energy cascade prevails for sufficiently weak rotation, estimated to manifest for Rossby numbers larger than $Ro \approx 0.1$. However, an important question that has not been answered clearly is whether or not the inclusion of rotation will impact the existing parameterizations for the irreversible mixing efficiency in unforced stably stratified flows that mostly do not account for the rotation.

Direct numerical simulations (DNS) have been an important avenue for understanding stratified turbulence both with and without the influence of rotation [5, 6, 8, 23, 30, 32, 33, 46, 47, 50, 53, 55, 56, 62]. Recent work using DNS has led to both some insights into and actual parameterizations of small-scale mixing [15, 29, 31, 37, 46, 47] by trying to answer questions about turbulent mixing in geophysical flows and demonstrating how DNS can be utilized in the broader study of geophysical flows. Some analysis of DNS of RST assert that there is an observable effect of rotation on the magnitude of potential energy available for mixing [46, 47]. Analysis of RST DNS has also shown that rotation and stratification are complementary in determining the relative strength of the direct and inverse energy cascades in the presence of forcing, when a dual energy cascade is detected [34, 48]. Here, we use decaying DNS simulations with rotation and stratification to help gain insight into irreversible (diapycnal) mixing and whether its inclusion in larger scale parameterizations of such mixing in stably stratified geophysical flows is needed for robust models.

Information and insights derived from numerical simulations is most useful when analyzed with thought to the complexity of laboratory and field observations. Applicability of any theoretical or numerical analysis is limited when it cannot be tested realistically or measured in a physical setting. However, making direct measurements of turbulent mixing in the field (in particular) is limited due to instrumentation capability and complications from internal wave motions that contaminate flux measurements [16, 60]. In oceanography, this has necessitated the use of indirect techniques to infer momentum and heat fluxes. The diapycnal diffusivity in an homogeneous and stationary flow is commonly defined in recent literature as:

$$\kappa_{\rho t} = \Gamma \frac{\epsilon}{N^2}, \quad \Gamma = \epsilon_P/\epsilon \tag{1}$$

where Γ is an irreversible mixing coefficient, ϵ_P is the rate of potential energy dissipation, ϵ is the rate of kinetic energy dissipation and $N = \sqrt{(-g/\rho_0)(d\langle\rho\rangle/dz)}$ is the buoyancy frequency with $\langle\rho\rangle$ denoting the horizontal average layer density. It is worth noting that the definition for $\kappa_{\rho t}$ given in Eq. 1 is consistent with the original definition provided by Osborn (1980) where $\kappa_{\rho t}$ was defined in terms of the flux Richardson number R_f since $\Gamma = R_f/(1 - R_f)$ [60]. All of the parameters in Eq. 1 are quantities that are readily available from a DNS. Determination of N and ϵ in the field requires simplifying assumptions such as local isotropy and choices on how the background density stratification is computed [4, 14], but it can generally be assumed that both N and ϵ are measurable in the physical setting. Γ is very commonly assumed to have a constant canonical value of 0.2, the upper limit proposed by [42]. The assumed constancy has been reviewed and challenged repeatedly [16]. Based on arguments in [60] the definition of the irreversible mixing coefficient Γ will be used exclusively herein. In addition, [60] highlight and discuss the importance of distinguishing between reversible processes (e.g. the inverse cascade before it reaches the size of the system when large-scale coherent structures will destabilize [40, 41]), and irreversible downscale processes (e.g. turbulent dissipation; [18, see *e.g.*]).

Parameterizations for the mixing efficiency in geophysical flows are commonly based on one of three fundamental dimensionless parameters: the Richardson number *Ri* [60]; the buoyancy Reynolds number Re_B [57, 58]; and the turbulent Froude number Fr_t [15, 31]. Rotational effects have not been included explicitly in the majority of mixing parameterizations of geophysical flows, presumably because rotational effects have been thought to not have a significant influence on dissipative processes. The ratio of the buoyancy frequency N to the Coriolis rotational frequency f has been a parameter of discussion related to types of expected turbulent mixing behavior, where the relative importance of this ratio on geostrophic lateral mixing has been discussed by various researchers in RST [24, 27, 46, 49, 62]. *N/f* has been thought to dictate the behavior of flow development, as for example the orientation of shear layers, but neither the turbulent Rossby number nor *N/f* control the amount of kinetic and potential energy dissipation in stably stratified flows (see [43] for a model, based on Reynolds averaging, of the possible influence of rotation on dissipation).

The limited effects of rotation on turbulent mixing in stably stratified flows have also been noted (e.g. see [13, 21] in the context of a modification to the Mellor-Yamada model), where effects of rotation impact regimes with convective or unstable flow dynamics. Establishing a clear picture of whether irreversible mixing is impacted by rotation in stably stratified geophysical flows, drives the present study. In what follows, a theoretical discussion on the key non-dimensional numbers is presented in section 2. Details of the numerical simulations and data are given in section 3 followed by the results in section 4 and conclusions in section 5, respectively.

2 Theoretical analysis

The amount of irreversible mixing in turbulent flows is a result of the dissipation of turbulent kinetic energy. The diapycnal (irreversible) mixing coefficient Γ, see Eq. 1, is an instantaneous measure of how much of the turbulent kinetic energy is converted to background potential energy through dissipation (e.g. see [10, 15, 20, 44, 63] for detailed discussion on the importance of Γ in stably stratified geophysical flows). The buoyancy

Reynolds number Re_B (also referred to as the Gibson number) is one of the most commonly used parameters for evaluating turbulent mixing since it can be calculated from field measurements (under certain assumptions such as isotropy at small scales) made in the atmosphere or ocean. In this context Re_B is commonly defined as

$$Re_B = \frac{\epsilon}{\nu N^2}, \tag{2}$$

where ν is the kinematic viscosity. However, despite its popularity, it has been noted that Re_B may be a useful but insufficient single parameter to characterize mixing [16, 36]. Definitional ambiguity comes from the possibility to achieve the same value for the buoyancy Reynolds through various combinations of its constituent parameters [37]. Note that the diapycnal diffusivity can be recast as a function of Re_B in non-dimensional form as

$$\frac{\kappa_{\rho t}}{\nu} = \Gamma Re_B. \tag{3}$$

Eq. 3 implies that Re_B needs to be sufficiently large for smaller-scale turbulence to exist [52]. It also shows how using Re_B to parameterize Γ might be ill-posed given that both of these quantities together define the diapycnal diffusivity. Given that the molecular diffusivities of scalars (salt and temperature) can vary by several orders of magnitude, it might be more appropriate to use a different dimensionless parameter for analyzing the degree of turbulent mixing of scalars as follows:

$$\hat{\kappa} = \frac{\kappa_{\rho t}}{\kappa} = \frac{\epsilon_P}{N^2 \kappa} = \Gamma Re_B Pr. \tag{4}$$

where κ is the molecular diffusivity of a scalar in a given fluid, and Pr is the molecular Prandtl (or Schmidt) number. Note that since $Pr = 1$ for all the simulations analyzed in this paper, the computation of parameters can be completed using either ν or κ. Values for this diffusivity ratio parameter $\hat{\kappa}$ are readily computable from the DNS results, but harder to obtain in the field, and illustrate the degree of separation between the molecular and turbulent scales.

The turbulent Froude number gives a ratio of buoyancy effects to turbulent effects in term of a ratio of timescales:

$$Fr_t = \frac{\epsilon}{Nk} \equiv \frac{1}{NT_L}, \tag{5}$$

where k is the turbulent kinetic energy and T_L is the turbulence time scale ($T_L = k/\epsilon$). Although there are a variety of ways to calculate the turbulent Froude number (see [2]), Fr_t as defined above may be the dimensionless parameter best suited to parameterize mixing in stratified turbulence [7, 20, 29, 58].

Difficulty in computing this number from measured quantities has limited its application in the field setting, but it has seen widespread use in numerical simulation analysis [30, 46]. Recent work has shown a link between the mixing efficiency and Fr_t [12, 15, 46]. The work by [15] is specifically designed to show how the link between Γ and Fr_t can be used by researchers analyzing data measured in the field. The degree of stratification and of turbulence are both contained in the definition of the turbulent Froude number and represent the two processes having the greatest influence on the evolution of the flow [29, 30]. In particular, the definition of the turbulent time scale $T_L = k/\epsilon$ is contained within this parameter, T_L being a measure of the decay time of turbulent kinetic energy [61]. In this

light, Fr_t can also be viewed as assessing the competition between the buoyancy time scale $\sim N^{-1}$ and the effective turbulent time scale T_L.

Analogous to the turbulent Froude number, the turbulent Rossby number defines the relative strength of rotational to turbulent effects, again, also in terms of time-scales:

$$Ro_t = \frac{\epsilon}{fk} = \frac{1}{fT_L}. \tag{6}$$

Using Fr_t and Ro_t as the two key parameters for the presentation of simulation results allows for evaluation of the relative impact of varied levels of stratification and rotation on the behavior of irreversible mixing in simulated geophysical flows. In Klymak et al [22], as well as in van Haren [17], one finds examples of geophysical flows with strong local intermittency where a lot of dissipation occurs amidst a quiet wave-dominated fluid (respectively Hawaii, and Puerto-Rico ridge), both relevant to the current work. We will initially present analysis using Re_B (Eq. 2), the common diagnostic parameter in stratified flow analysis. The analysis will be extended to use of $\hat{\kappa}$ (Eq. 4) as the key diagnostic parameter to both evaluate and ensure that small-scale irreversible mixing does indeed exist in the analysis of DNS data, as it gives a direct measure of the separation between the molecular and turbulent scales. If the molecular diffusivity, κ, in a simulation is of greater or equal magnitude to the diapycnal diffusivity, $\kappa_{\rho t}$, no physically realistic irreversible mixing is occurring.

3 Simulations and data

Direct numerical simulations of the Navier–Stokes equations with the Boussinesq approximation and with rotation, Eqs. 7 and 8, were made using the Geophysical High-Order Suite for Turbulence (GHOST) code (see [38] for details). GHOST is a pseudo-spectral computational fluid framework that is parallelized using a hybrid MPI/OpenMP/CUDA scheme and has demonstrated excellent scalability and performance to over 130,000 computational nodes [54].

$$\partial_t \mathbf{u} - \nu \Delta \mathbf{u} + N\theta \hat{z} + \nabla p - f\mathbf{u} \times \hat{z} = -\mathbf{u} \cdot \nabla \mathbf{u} \tag{7}$$

$$\partial_t \theta - \kappa \Delta \theta - Nw = -\mathbf{u} \cdot \nabla \theta \tag{8}$$

All simulations were made using $n_P = 1024^3$ grid points in a triply periodic box (see Table 1). How well a simulation is resolved is classically determined by the ratio of the dissipative scale η to the smallest resolved scale $k_{max} = n_P^{1/3}/3$, assuming a quadratic non-linearity and with $1 \lesssim \eta k_{max}$ [45]. A classical turbulent (Kolmogorov) spectrum yields $\eta = [\epsilon/\nu^3]^{-1/4}$ by assuming equality between the linear dissipation time and the eddy turn-over time at scale η. This expression is used here even when no fully developed turbulent spectrum has been obtained due to the presence of strong waves at low Froude number (see *e.g.* Legaspi and Waite [25], de Bruyn Kops [23], Maffioli and Davidson [30], Rosenberg et al [54], Kurien and Smith [24], Marino et al [33] for spectral studies of stratified flows with and without rotation). Note that the six runs (20% of the data set) that are least resolved, in the sense that ηk_{max} is quite close to unity (from above), have the lowest Re_B, making these runs in the range of flows dominated by waves (at the edge of regime I of Pouquet et al [46]). This result is *a priori* surprising since these low Re_B flows are

ostensibly less turbulent and should therefore require lower resolution than the higher Re_B runs. This seeming contradiction can be understood by recalling that strong large-scale intermittency results at the onset of the regime of eddy-wave competition [12], leading to a need for increased numerical resolution.

Simulations 1-10 in Table 1 all have velocity initialized at large scales with Taylor-Green vortices (TG hereafter), with $\mathbf{u}_{TG} = [sin(x)cos(y)cos(z)\hat{e}_x, -cos(x)sin(y)cos(z)\hat{e}_y, 0\hat{e}_z]$; this flow has been utilized as well in other studies of stratified flows [19, 50, 59]. Initialization with Taylor-Green vortices primes the development of strong internal shear layers and of rotational flow structures within a simulation, rather than having rotational structures forced to develop from random initial conditions. These structures were allowed to evolve naturally in the absence of forcing. The impact of rotation on the irreversible mixing coefficient should be most apparent in these ten simulations if it is influencing scalings via Fr_t and Ro_t.

Simulations 11-30 are initialized with randomized phases in Fourier space. These twenty simulations are a subset of the randomly initialized runs previously presented and analyzed in Pouquet et al [46], Rosenberg et al [55]. There are no initial scalar fluctuations with either initialization. This setup allows for the buoyancy fluctuations to develop from the internal dynamics of the Boussinesq equations [55]. Inputs to all simulations were varied by specification of the buoyancy frequency N, Coriolis rotation f, kinematic viscosity v, molecular diffusivity κ (always maintaining a Prandtl number, $Pr = v/\kappa$, equal to 1) and the evolutionary time step. No mean shear or other forcing was imposed in the simulations;
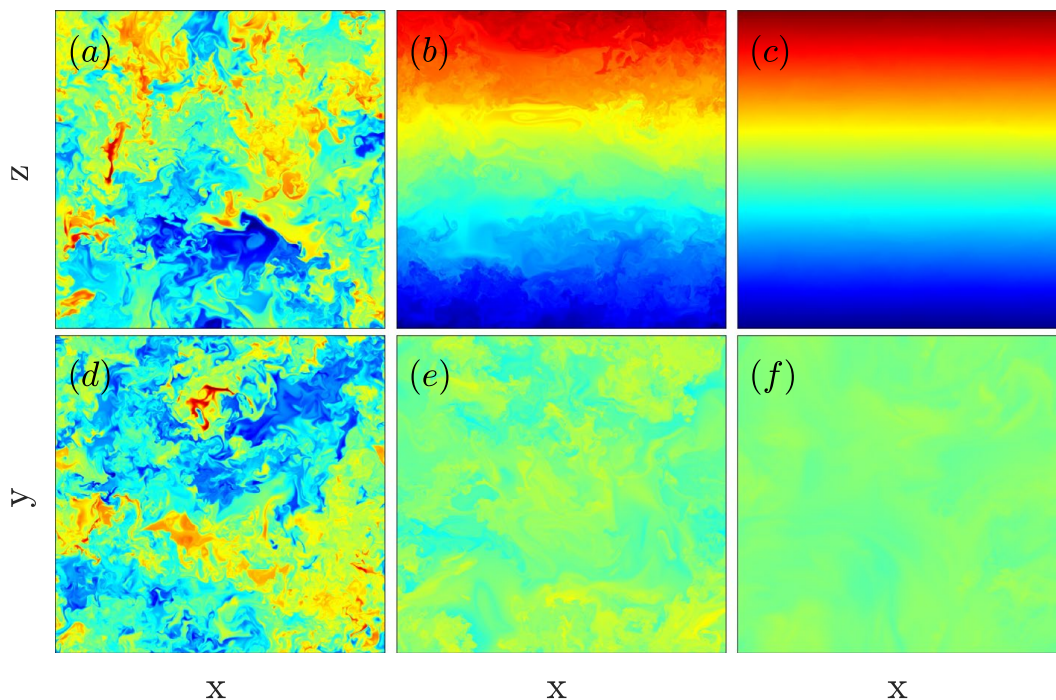
Fig. 1 The first row (panels *a-c*) shows vertical plane visualizations of three simulations using the scalar field in the center ($y = \pi$) near the peak of dissipation. All three simulations have the same rotational frequency ($f = 0.04$) but the stratification increases from left to right, $N = 0.2$, $N = 1.6$ and $N = 5.5$ (run 14, 18 and 22 respectively, see Table 1). The corresponding turbulent Froude numbers vary altogether by two orders of magnitude. The red-to-blue colors represent the continual change from lighter to heavier fluid. The second row (panels *d -f*) depicts a horizontal plane ($z = \pi$) visualization of the same field in the center of the box for the same runs

Table 1 Details of the 30 simulations, where the turbulent Froude, turbulent Rossby and buoyancy Reynolds numbers are calculated at the peak of the dissipation rate of total turbulent energy.

Run	$N(s^{-1})$	$f(s^{-1})$	N/f	Fr_t	Ro_t	Re_B	Re_0	ηk_{max}	JFM ID
1	0.7	0.13	5	0.78	3.87	791	2222	1.34	–
2	5.0	1.00	5	0.06	0.31	10	3333	1.17	–
3	2.7	0.38	7	0.13	0.91	59	4000	1.22	–
4	0.4	0.02	20	1.54	30.75	12740	10000	1.31	–
5	0.5	0.40	1.25	1.22	1.53	5004	6667	1.32	–
6	1.0	0.80	1.25	0.49	0.62	894	5714	1.31	–
7	2.0	1.60	1.25	0.20	0.25	254	8000	1.24	–
8	1.0	1.00	1	0.50	0.50	1057	6667	1.25	–
9	1.0	0.40	2.5	0.60	1.50	1279	6667	1.26	–
10	2.5	0.25	10	0.27	2.56	263	8000	1.24	–
11[1]	1.0	0.01	106	0.28	30.03	110	1818	1.29	JFM54
12[1]	1.9	0.01	199	0.11	22.39	27	1818	1.28	JFM37
13[1]	0.1	0.04	2.5	4.25	10.62	48886	3704	1.37	JFM61
14[1]	0.2	0.04	5	2.035	10.18	10851	3704	1.36	JFM60
15[1]	0.4	0.04	10	1.034	10.34	4035	6494	1.34	JFM59
16[1]	0.8	0.04	20	0.473	9.46	893	6494	1.33	JFM56
17[1]	1.2	0.04	30	0.29	8.56	384	6667	1.33	JFM53
18[1]	1.6	0.04	40	0.18	7.11	194	6667	1.30	JFM51
19[1]	2.0	0.04	50	0.13	6.30	110	6667	1.25	JFM49
20[1]	2.4	0.04	60	0.09	5.36	69	6667	1.24	JFM46
21[1]	3.8	0.04	94	0.04	3.43	20	6667	1.18	JFM39
22[1]	5.5	0.04	138	0.02	2.11	6	6667	1.11	JFM31
23[1]	3.8	0.05	69	0.04	2.57	30	10000	1.20	JFM41
24[1]	2.0	0.04	25	0.13	3.13	109	6667	1.30	JFM48
25[1]	4.0	0.08	50	0.03	1.60	16	6667	1.14	JFM35
26[1]	0.7	0.27	2.6	0.53	1.33	817	4762	1.33	JFM57
27[1]	1.3	0.54	2.5	0.24	0.58	200	4762	1.26	JFM52
28[1]	2.7	0.54	4.9	0.07	0.33	34	4762	1.25	JFM43
29[1]	3.8	0.75	5.0	0.03	0.16	17	4762	1.19	JFM33
30[1]	2.7	1.07	2.5	0.06	0.14	29	4762	1.27	JFM42

The initial Reynolds number is given by $Re_0 = U_0 L_0 / \nu$ with the initial characteristic length and velocity scales $L_0 = 1$ and $U_0 = 1$ respectively, hence $\nu \equiv 1/Re_0$. Superscript [1] in the first column denotes a data subset also analyzed in [46] (with identification ID). Note that Fr_t can be computed directly from Ro_t and N/f. Finally, ηk_{max} is a measure of how well a simulation has been resolved [45]. See discussion in text

hence, the energy decays over the course of a simulation. Thus, a total of thirty DNS runs using the GHOST code are presented and evaluated to study the effect of rotation on irreversible mixing. Table 1 gives the details of all simulations in this analysis.

Figure 1 shows two-dimensional snapshots of 3 different simulations at or near the peak of dissipation rate of turbulent kinetic energy in the vertical plane at the center ($y = \pi$) of the periodic box (panels a–c), or in the horizontal plane ($z = \pi$, panels d–f).

The snapshots of the vertical cross-sections show the instabilities of the flow using the scalar field for runs 14, 18 and 22. The simulations in panels *a–f* have the same imposed rotation ($f = 0.04$) but the stratification increases from left to right. It is clear from these visualizations that turbulent eddies decrease in intensity with increasing stratification. Note that the Reynolds numbers of these runs vary by at most a factor of 2, whereas Re_B varies by roughly three orders of magnitude: Neither Re nor Re_B is as good a predictor of the behavior of these flows as $\hat{\kappa}$, a point that will be examined in more detail in the following section emphasizing the importance of the (turbulent) Froude number.

4 Results

4.1 Energy and dissipation

Influences of rotation are commonly visible in geophysical flows at the energy containing scales. Examples of the evolution of simulation volume integrated kinetic energy and dissipation rate are given in Fig 2 (see [55] for description and calculations of all quantities). Fig 2a shows the evolution of kinetic energy of run 14 (dashed lines), run 18 (dash-dot lines) and run 22 (dotted lines), respectively. Fig 2c, e show the evolution of potential energy and the kinetic energy dissipation rate, respectively for the same three runs presented in Fig 2a. Dissipation rates for these simulations were calculated using simulation enstrophy (see [38, 46, 55] for details on the calculations of all diagnostics). These are the same simulations visualized in rows one and two of Fig 1. As the stratification increases there is a visible increase in the oscillatory transfer of energy between the kinetic (green)
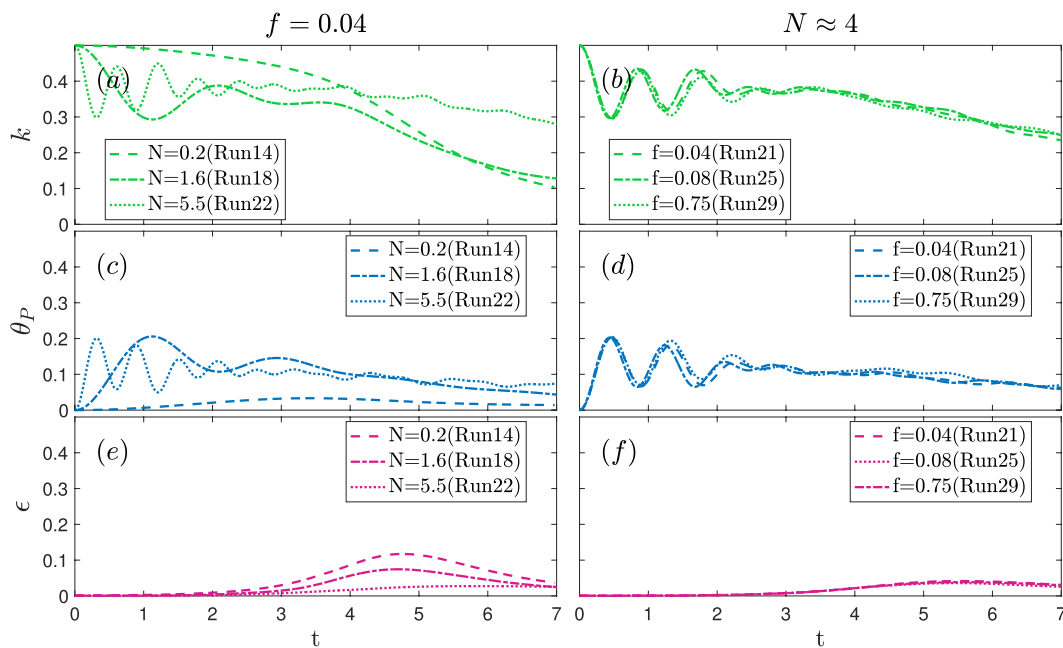

Fig. 2 Temporal evolution of volume-integrated kinetic energy k (green), potential energy θ_P (blue), and kinetic energy dissipation rate ϵ (magenta) for runs at a constant rotation $f = 0.04$ (1st column, panels *a*, *c* and *e*) and at approximately constant stratification, $N = 3.8 - 4.0$ (2nd column, panels *b*, *d* and *f*, see Table 1)

and potential (blue) modes ($\theta_P = \langle \theta^2/2 \rangle$). It is also clear that increases in stratification lowers the turbulent dissipation rate (magenta). Figure 2b, Figure 2d, f show the same quantitative evolutions but for simulations runs 21, 25 and 29 where the buoyancy frequency of the simulations are similar ($N = 3.8 - 4.0$) between the runs and the value for f is varied. Unlike variations of N, variations of f do not significantly influence the behavior of energy or dissipation rate in the simulations. These results are consistent with the results of simulation runs 9, 6 and 8 (not shown here) where $N = 1$ in all three simulations but rotation of the runs is $f = 0.4$, $f = 0.8$ and $f = 1$ respectively. It is apparent from these simple diagnostics that f does not appear to have a noticeable influence on the energetics (especially on the dissipation rates) in unforced stably stratified flows. Clearly the rotational parameter is an order of magnitude, or less, than the buoyancy parameter for the runs in Fig 2b. This likely limits the influence of f as compared to N on the flow. The relative magnitudes of these parameters in the simulations was chosen in order to maintain their relevance to N/f values seen in geophysical flows and will be explained in more detail in the following section.

4.2 Parametric space

Figure 3 plots a portion of time series data from all 30 of the runs analyzed in this study as discrete values. Data plotted for each run shows parameter values at 12 different times starting at the time of the peak of the dissipation rate. These 12 data points are equally time-spaced values over this interval with the intermediate between each point simply removed for visualization. These sub-sets of the data are presented in a Fr_t-Ro_t parametric framework. The runs can be easily distinguished. They all evolve from a higher to a lower value of Re_B, because of self-similar energy dissipation (see [53] for the purely stratified case). Within this framework the temporal evolution of any given simulation, as expected,
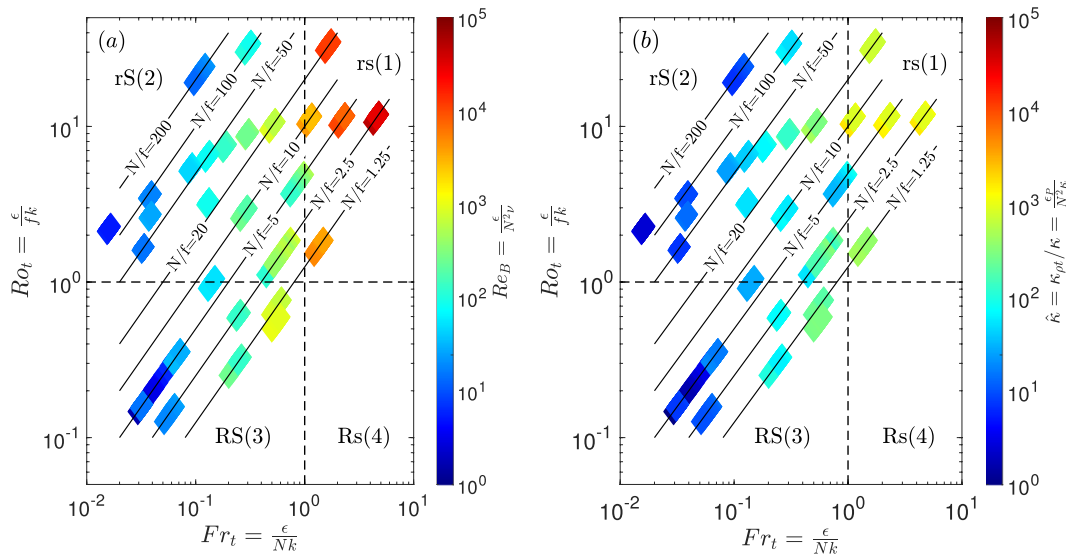
Fig. 3 Time series plots of the runs in a parametric framework using Fr_t and Ro_t. Data is colored by Re_B (**a**) and by the diffusivity ratio $\hat{\kappa}$ (**b**), see Eqs. 2 and 4, respectively. Note that $Pr = 1$ for all simulations and $\hat{\kappa} = \kappa_{pt}/\kappa = \Gamma Re_B Pr$. The use of $\hat{\kappa}$ eliminates the ambiguity associated with referring simply to Re_B; it gives a clear depiction of molecular and turbulent scale separation and should be used for evaluating DNS data, ensuring physically realistic flows

follows the lines of constant N/f. Also, the magnitudes of Fr_t and Ro_t evolve over the course of the simulations due to turbulent dissipation. As the magnitudes of Ro_t and Fr_t decrease, the increase in stratification will limit the amount of turbulence and mixing, especially vertically (see Fig. 1).

Work presented by Mater and Venayagamoorthy [37] uses a multiple parameter framework to evaluate the dominant flow regimes in stratified shear flows by comparing buoyancy and shear strength parameters. This new parametric framework uses the same idea, defining now dominant flow regimes that include rotation but with an absence of imposed shear (and of forcing). Thus, in a framework comparing Ro_t against Fr_t Fig. 3 clearly shows how the relative magnitudes of rotation and stratification are coupled in the geophysical context along lines of constant N/f. All flows in this parametric space evolve, as noted above, where values of $N/f \sim 100$ are commonly seen in the atmosphere and $N/f \lesssim 10$ is appropriate for the oceanic setting.

The parametric space is divided into four different regions using $O(1)$ magnitudes of Fr_t and Ro_t as delineations and the nomenclature of [3] for classification. These delineations simply denote the relative strength/magnitude of N as compared to f and are not necessarily based on *a priori* changes in the flow physics. It can certainly be observed that some simulations evolve dynamically from one region to another. In region 1, the magnitudes of the rotation and stratification are small and of comparable magnitude, so this quadrant of the graph is denoted by *rs*. While there is an influence of stratification and rotation in this region, the flow behavior likely approximates the behavior of classical turbulence since their effects are negligible (i.e. high Fr_t and high Ro_t). In region 2, the stratification is approximately an order of magnitude greater than the rotation and is denoted rS (low Fr_t, high Ro_t). Rotation and stratification are both significant and have similar magnitudes in region 3, RS. Region 4 denotes an area in the parametric framework where the rotation is at least an order of magnitude greater than the stratification, Rs.

The majority of geophysical flows are classified as falling along one of the N/f lines denoted before, therefore none of the simulations fall into region 4 where $N/f < 1$. Flows that fall into this classification region may be relevant in astrophysics, for example for stars that are rotating rapidly, but are not seen except in specific isolated cases in the geophysical setting. The magnitude of rotation in all simulations here ($Ro_t \geq 0.1$) is such that such flows would be considered weakly rotating except in certain specific contexts (i.e. [11]). Increasing the amount of rotation to reach an order of magnitude where $Ro_t \leq 0.01$ and maintaining N/f relevant to the geophysical setting would also necessitate an increase in N, which would lead to simulations with too high a stratification to generate turbulence without a significant increase in the Reynolds number of a simulation, which is computationally costly.

Data in Fig. 3a is colored by the buoyancy Reynolds number in order to illustrate one of the common measures of turbulent mixing. In the plots, values for the buoyancy Reynolds number are limited to $O(1)$ or greater, which eliminates inclusion of viscosity-affected (low Reynolds number) flows. From these results, it can be easily seen that the ratio of N/f is not a useful diagnostic tool for explicitly determining levels of turbulent mixing. Re_B values vary by up to three orders of magnitude on multiple N/f lines. Additionally, the turbulent Froude number can also be observed to take almost any value in the rS and RS regimes for any given N/f. These observations point to the fact that while both N and f influence the flow, it is clear that their ratio does not provide a diagnostic signature for the levels of irreversible mixing in RST in the absence of forcing.

Figure 3b gives the same data as in Fig. 3a, but colored now by the diffusivity ratio $\hat{\kappa}$ whose values are also constrained to $O(1)$ or greater in order to exclude data dominated

by molecular mixing effects. $\hat{\kappa}$ is a useful parameter as it gives a measure of the separation between the molecular and turbulent scales that eliminates the definitional ambiguity that arises from use of Re_B which combines turbulent dissipation and stratification in one sole parameter. DNS results that do not report a value for $\hat{\kappa}$ that is at least $O(1)$ have mixing mostly, if not exclusively, due to molecular diffusion. It has been shown that the background mixing in the ocean is of $O(10)$ [39] and these simulations have been designed to be comparable to physically realistic flows. In other words, DNS runs where $\hat{\kappa} < O(1)$ may introduce non-physical data where the molecular diffusion is the same order of magnitude, or larger, than the turbulent diffusion. Run 22 is an example of a run that is near this threshold and included here as an example. Some of the results in this plot show values for $\hat{\kappa}$ that would suggest limited amounts of mixing when compared to the data evaluated using Re_B that suggest more significant levels of mixing, highlighting the fact that evaluation using Re_B may give an impression of more elevated mixing than what is actually present. This further illustrates the importance of using multiple parameters and criteria for the evaluation of mixing in DNS data. This theoretical framework based on (Fr_t, Ro_t) provides a useful diagnostic for classifying RST DNS for geophysical flow regimes and could also be applied to measured data if parameterizations to determine Fr_t from measurable quantities are used as proposed by Garanaik and Venayagamoorthy [15].

4.3 Irreversible mixing

Figure 4 presents the parameterization of Γ as function of Fr_t for the RST runs plotted together with the non-rotating DNS data presented in Garanaik and Venayagamoorthy [15]: sheared unstratified Shih et al [58], forced stratified [31] and unforced stratified runs [15]. The remarkable feature is that the scaling relationship between Γ and Fr_t presented in Garanaik and Venayagamoorthy [15] holds well despite the fact that f does not appear explicitly in Fr_t. An increase in the irreversible mixing efficiency for $Fr_t \sim 0.1$ seen in
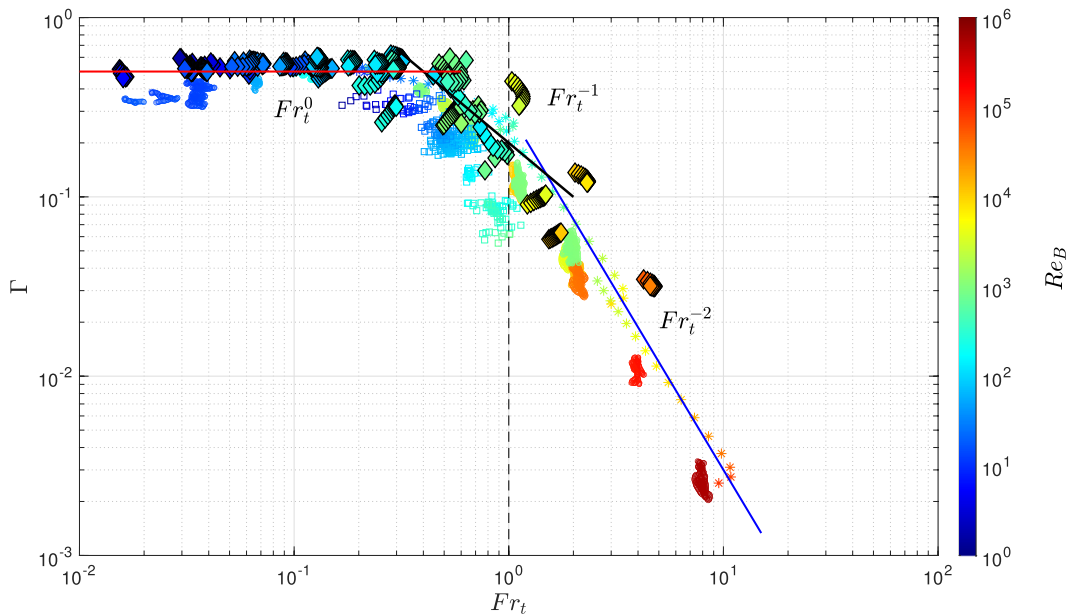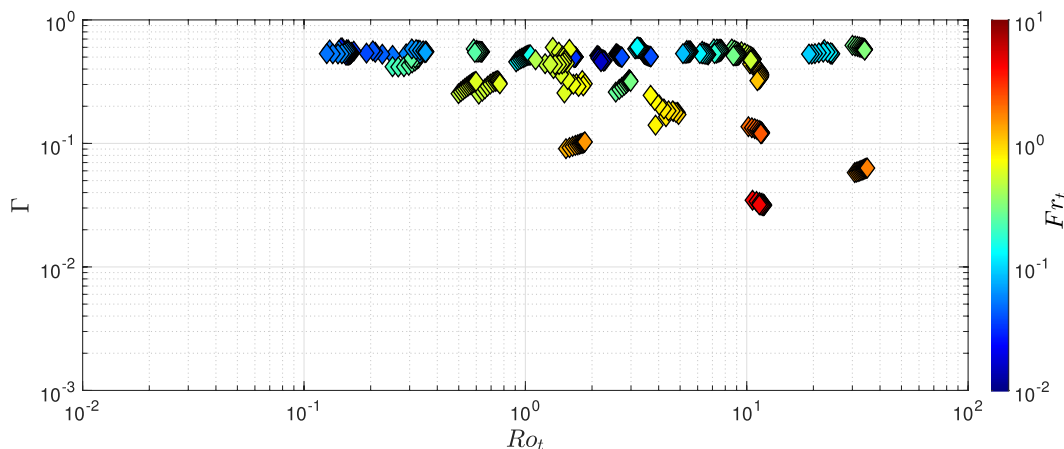

Fig. 4 Irreversible mixing coefficient Γ defined in Eq. (1) as a function of turbulent Froude number Fr_t. The color bar at right indicates values of Re_B. Diamond: decaying RST DNS; star: decaying stratified turbulence [15]; circle: forced DNS [31]; square: sheared DNS data [58]

some studies is not observed here (e.g. [31]). While the presence of rotation may provide additional energy at scales comparable to and larger than the energy-containing scales in a stratified flow, it does not appear to have any discernible effect on the scaling of the diapycnal (small-scale) irreversible mixing coefficient, at least at these Reynolds numbers. It can also be seen in Fig. 4 that the distribution of Re_B covers six orders of magnitude and that, more importantly, Re_B can vary by over an order of magnitude for any given value of Γ, reinforcing previous research showing the ambiguity of Re_B. As previously noted in Garanaik and Venayagamoorthy [15] it is clear that a unique scaling of Γ with Re_B is not possible. These results extend the observations presented in Garanaik and Venayagamoorthy [15] to data that includes the influence of rotation. While the present analysis focuses on the inclusion of f into evaluation of the mixing coefficient Fig. 4 shows the same Γ scaling for sheared, forced, unforced and rotating in DNS data. This figure shows that all of these conditions do not appear to influence irreversible mixing when taken individually.

Finally, Fig. 5 presents the parameterization of Γ as a function of the second dynamic turbulent parameter investigated here, Ro_t, with coloring of data points depending on Fr_t. Data in this figure further emphasize that rotation does not have a strong influence on the irreversible mixing, as there is no clear scaling between Ro_t and Γ. Indeed, Γ is seen to be roughly constant, except when both the turbulent Rossby and Froude numbers are larger than unity. Additionally, there are no clear groupings of simulations of similar magnitude in Ro_t solely based on the magnitude of Fr_t.

5 Concluding remarks

This paper analyzes scaling properties of homogeneous, decaying and rotating stratified turbulent mixing through the irreversible mixing parameter Γ. A new parametric framework using Fr_t and Ro_t is used to show how the relative magnitudes of rotation and stratification present in geophysical flow regimes of the Earth's ocean and atmosphere affect flow statistics. DNS data is plotted within this framework using Re_B, and more importantly $\hat{\kappa}$ as diagnostics of the degree of irreversible turbulent mixing. The diffusivity ratio $\hat{\kappa}$ in the simulations is realistic for observed physical values and is suggested as a more robust parameter than Re_B for evaluating the degree of mixing in DNS by illustrating the

Fig. 5 Irreversible mixing coefficient Γ as a function of turbulent Rossby number Ro_t for simulations presented in this manuscript that included rotation. The color bar at right indicates values of Fr_t

degree of separation between the turbulent and molecular scales. Variations in Re_B and $\hat{\kappa}$ for any given value of N/f clearly show that N/f does not have any unique relationship to the amount of diapycnal mixing in stable decaying RST. Significant variations in the magnitude of both Fr_t and Ro_t for any given N/f are also observed, supporting this conclusion. RST data from this study plotted with non-rotating but stratified DNS data show remarkable agreement in the scaling relationship between the irreversible mixing coefficient and the turbulent Froude number.

Rotation has been clearly observed to influence the large-scale flow structures that develop in some geophysical flows and simulations. The inclusion of rotation may also influence kinetic and potential dissipation rates individually. However, rotation does not appear to have a direct influence on their ratio, the irreversible mixing efficiency parameter in the absence of forcing. Additionally, it is clear from this analysis that existing parameterizations between the irreversible mixing coefficient Γ and the turbulent Froude number Fr_t are applicable to unforced rotating stratified turbulence.

References

1. Aguilar DA, Sutherland BR (2006) Internal wave generation from rough topography. Phys Fluids 18(6):066–603
2. Almalkie S, de Bruyn Kops SM (2012) Kinetic energy dynamics in forced, homogeneous, and axisymmetric stably stratified turbulence. J Turbul 13:N29
3. Aluie H, Kurien S (2011) Joint downscale fluxes of energy and potential enstrophy in rotating stratified Boussinesq flows. Europhys Lett 96(4):44006
4. Arthur RS, Venayagamoorthy SK, Koseff JR et al (2017) How we compute N matters to estimates of mixing in stratified flows. J Fluid Mech. https://doi.org/10.1017/jfm.2017.679
5. Bartello P (1995) Geostrophic adjustment and inverse cascade in rotating stratified turbulence. J Atmos Sci 52:4410–4428
6. Bartello P, Métais O, Lesieur M (1996) Geostrophic versus wave eddy viscosities in atmospheric models. J Atmosph Sci 53:564–571
7. Brethouwer G (2005) The effect of rotation on rapidly sheared homogeneous turbulence and passive scalar transport. Linear theory and direct numerical simulation. J Fluid Mechs 542:305–342
8. Brethouwer G, Billant P, Lindberg E et al (2007) Scaling analysis and simulation of strongly stratified turbulent flows. J Fluid Mech 585:343–368
9. Cambon C, Godeferd FS, Nicolleau F et al (2004) Turbulent diffusion in rapidly rotating flows with and without stable stratification. J Fluid Mech 499:231–255
10. Caulfield CP (2021) Layering, instabilities, and mixing in turbulent stratified flows. Ann Rev Fluid Mech 53:113–145
11. Ecke RE, Niemela JJ (2014) Heat transport in the geostrophic regime of rotating Rayleigh-Benard convection. Phys Rev Lett 113(11):114–301
12. Feraco F, Marino R, Pumir A et al (2018) Vertical drafts and mixing in stratified turbulence: sharp transition with Froude number. Europhys Lett 123(4):44002
13. Galperin B, Kantha L, Mellor G et al (1989) Modeling rotating stratified turbulent flows with application to oceanic mixed layers. J Phys Oceanograp 19(7):901–916
14. Garanaik A, Venayagamoorthy SK (2018) Assessment of small-scale anisotropy in stably stratified turbulent flows using direct numerical simulations. Phys Fluids 30(126):602

15. Garanaik A, Venayagamoorthy SK (2019) On the inference of the state of turbulence and mixing efficiency in stably stratified flows. J Fluid Mech 867:323–333
16. Gregg MC, D'Asaro E, Riley JJ et al (2018) Mixing efficiency in the ocean. Annual Rev Marine Sci 10:443–473
17. van Haren H (2017) Aabw-transport variation and its effect on internal wave motions between top and bottom of the Puerto Rico trench. J Marine Res 75(4):507–529
18. Hasselmann K (1963) On the non-linear energy transfer in a gravity-wave spectrum. Part 2. Conservation theorems; wave-particle analogy; irreversibility. J Fluid Mech 15:273–281
19. Hebert D, de Bruyn Kops SM (2006) Relationship between vertical shear rate and kinetic energy dissipation rate in stably stratified flows. Geophys Res Lett 33(L06):602
20. Ivey GN, Imberger J (1991) On the nature of turbulence in a stratified fluid. Part I: the energetics of mixing. J Phys Oceanogr 21(5):650–658
21. Kantha L, Rosati A, Galperin B (1989) Effect of rotation on vertical mixing and associated turbulence in stratified fluids. J Geophys Res: oceans 94(C4):4843–4854
22. Klymak JM, Moum JN, Nash JD et al (2006) An estimate of tidal energy lost to turbulence at the hawaiian ridge. J Phys Oceanogr 36(6):1148–1164
23. de Bruyn Kops SM (2019) The effects of stable stratification on the decay of initially isotropic homogeneous turbulence. J Fluid Mech 860:787–821
24. Kurien S, Smith LM (2014) Effect of rotation and domain aspect-ratio on layer formation in strongly stratified Boussinesq flows. J Turbul 15(4):241–271
25. Legaspi JD, Waite ML (2020) Prandtl number dependence of stratified turbulence. J Fluid Mech. https://doi.org/10.1017/jfm.2020.619
26. Lelong MP, Dunkerton TJ (1998) Inertia-gravity wave breaking in three dimensions. Part i: convectively stable waves. J Atmos Sci 55(15):2473–2488
27. Lelong MP, Sundermeyer MA (2005) Geostrophic adjustment of an isolated diapycnal mixing event and its implications for small-scale lateral dispersion. J Phys Oceanogr 35(12):2352–2367
28. Lindborg E (2005) The effect of rotation on the mesoscale energy cascade in the free atmosphere. Geophys Res Lett 32:1–4
29. Lindborg E, Brethouwer G (2008) Vertical dispersion by stratified turbulence. J Fluid Mech 614:303–314
30. Maffioli A, Davidson PA (2016) Dynamics of stratified turbulence decaying from a high buoyancy reynolds number. J Fluid Mech 786:210–233
31. Maffioli A, Brethouwer G, Lindborg E (2016) Mixing efficiency in stratified turbulence. J Fluid Mech 794:R3
32. Marino R, Mininni PD, Rosenberg D et al (2013) Inverse cascades in rotating stratified turbulence: fast growth of large scales. Europhys Lett 102(4):44006
33. Marino R, Mininni PD, Rosenberg D et al (2014) Large-scale anisotropy in stably stratified rotating flows. Phys Rev E 90(023):018
34. Marino R, Pouquet A, Rosenberg D (2015) Resolving the paradox of oceanic large-scale balance and small-scale mixing. Phys Rev Lett 114(11):114–504
35. Marino R, Rosenberg D, Herbert C et al (2015) Interplay of waves and eddies in rotating stratified turbulence and the link with kinetic-potential energy partition. EuroPhys Lett 112(49):001
36. Mater BD, Venayagamoorthy SK (2014) The quest for an unambiguous parameterization of mixing efficiency in stably stratified geophysical flows. Geophys Res Lett 41(13):4646–4653
37. Mater BD, Venayagamoorthy SK (2014) A unifying framework for parameterizing stably stratified shear-flow turbulence. Phys Fluids 26(3):036–601
38. Mininni PD, Rosenberg D, Reddy R et al (2011) A hybrid MPI-OpenMP scheme for scalable parallel pseudospectral computations for fluid turbulence. Parallel Computing 37(6–7):316–326
39. Munk W, Wunsch C (1998) Abyssal recipes II: energetics of tidal and wind mixing. Deep Sea Res Part I: oceanogr Res Papers 45(12):1977–2010
40. Newell A, Zakharov V (2008) The role of the generalized Phillips spectrum in wave turbulence. Phys Lett A 372:4230–4233
41. Newell A, Nazarenko S, Biven L (2001) Wave turbulence and intermittency. Physica D 152–153:520–550
42. Osborn TR (1980) Estimates of the local rate of vertical diffusion from dissipation measurements. J Phys Oceanogr 10(1):83–89
43. Park JY, Chung MK (1999) A model for the decay of rotating homogeneous turbulence. Phys Fluids 11:1544–1560
44. Peltier WR, Caulfield CP (2003) Mixing efficiency in stratified shear flows. Annual Rev Fluid Mech 35:135–167

45. Pope SB (2000) Turbulent flows. Cambridge University Press, Cambridge
46. Pouquet A, Rosenberg D, Marino R et al (2018) Scaling laws for mixing and dissipation in unforced rotating stratified turbulence. J Fluid Mech 844:519–545
47. Pouquet A, Rosenberg D, Marino R (2019) Linking dissipation, anisotropy, and intermittency in rotating stratified turbulence at the threshold of linear shear instabilities. Phys Fluids 31(10):105–116
48. Pouquet A, Rosenberg D, Stawarz JE et al (2019) Helicity dynamics, inverse, and bidirectional cascades in fluid and magnetohydrodynamic turbulence: a brief review. Earth Space Sci 6:351
49. Praud O, Sommeria J, Fincham A (2006) Decaying grid turbulence in a rotating stratified fluid. J Fluid Mech 547:389–412
50. Riley JJ, de Bruyn Kops SM (2003) Dynamics of turbulence strongly influenced by buoyancy. Phys Fluids 15(7):2047–2059
51. Riley JJ, Lelong MP (2000) Fluid motions in the presence of strong stable stratification. Annual Rev Fluid Mech 32:613–657
52. Davidson PA, Kaneda Y, Sreenivasan KR (2013) Ten chapters in turbulence. Cambridge University Press, Cambridge, England, U.K., pp 437
53. Rorai C, Mininni PD, Pouquet A (2015) Stably stratified turbulence in the presence of large-scale forcing. Phys Rev E 92(1):013003
54. Rosenberg D, Pouquet A, Marino R et al (2015) Evidence for Bolgiano-Obukhov scaling in rotating stratified turbulence using high-resolution direct numerical simulations. Phys of Fluids 27(5):055–105
55. Rosenberg D, Marino R, Herbert C et al (2016) Variations of characteristic time scales in rotating stratified turbulence using a large parametric numerical study. Eur Phys J E 39(1):8
56. Rosenberg D, Marino R, Herbert C et al (2017) Correction to: variations of characteristic time scales in rotating stratified turbulence using a large parametric numerical study. Eur Phys J E 40(10):87
57. Salehipour H, Peltier WR (2015) Diapycnal diffusivity, turbulent Prandtl number and mixing efficiency in Boussinesq stratified turbulence. J Fluid Mech 775:464–500
58. Shih LH, Koseff JR, Ivey GN et al (2005) Parameterization of turbulent fluxes and scales using homogeneous sheared stably stratified turbulence simulations. J Fluid Mech 525:193–214
59. Sujovolsky N, Mininni P, Pouquet A (2018) Generation of turbulence through frontogenesis in sheared stratified flows. Phys Fluids 30(086):601
60. Venayagamoorthy SK, Koseff JR (2016) On the flux Richardson number in stably stratified turbulence. J Fluid Mech 798:R1
61. Venayagamoorthy SK, Stretch DD (2010) On the turbulent Prandtl number in homogeneous stably stratified turbulence. Journal of Fluid Mechanics 644:359–369
62. Waite ML, Bartello P (2006) The transition from geostrophic to stratified turbulence. Journal of Fluid Mechanics 568:89–108
63. Winters KB, Lombard PN, Riley JJ et al (1995) Available potential energy and mixing in density-stratified fluids. Journal of Fluid Mechanics 289:115–128

Authors and Affiliations

Matthew Klema[1,2] [ID] **· S. Karan Venayagamoorthy[1] · Annick Pouquet[3,4] ·
Duane Rosenberg[5] · Raffaele Marino[6]**

S. Karan Venayagamoorthy
vskaran@colostate.edu

Annick Pouquet
pouquet@ucar.edu

Duane Rosenberg
duaner62@gmail.com

Raffaele Marino
raffaele.marino@ec-lyon.fr

[1]   Civil and Environmental Engineering Department, Colorado State University, Fort Collins, CO 80523, USA

[2]   Department of Physics and Engineering, Fort Lewis College, Durango, CO 81301, USA

[3]   Laboratory for Atmospheric and Space Physics, University of Colorado, Boulder, CO 80309, USA

[4]   National Center for Atmospheric Research, P.O. Box 3000, Boulder, CO 80307, USA

[5]   Cooperative Institute for Research in the Atmosphere, NOAA, G/GSD, 325 Broadway, Boulder, CO 80305, USA

[6]   Laboratoire de Mécanique des Fluides et d'Acoustique, UMR5509, F-69134, Université de Lyon, CNRS, École Centrale de Lyon, INSA Lyon, Université Claude Bernard Lyon 1, 69134 Écully, France